

Template-directed Bifunctional NiS_x/Nitrogen-doped Mesoporous Carbon Electrocatalyst for Rechargeable Zn–air Batteries

Kai Wan,[†] Jiangshui Luo,^{†,‡,§} Xuan Zhang,^{*†} Chen Zhou,[†] Jin Won Seo,[†] Palaniappan Subramanian,[†] Jia-wei Yan,[§] and Jan Fransaer^{*†}*

[†]Department of Materials Engineering, KU Leuven, Leuven 3001, Belgium.

[§]Collaborative Innovation Center of Clean Energy, Longyan University, Longyan 364012, China.

[§]State Key Laboratory of Physical Chemistry of Solid Surfaces and Department of Chemistry, College of Chemistry and Chemical Engineering, Xiamen University, Xiamen 361005, China.

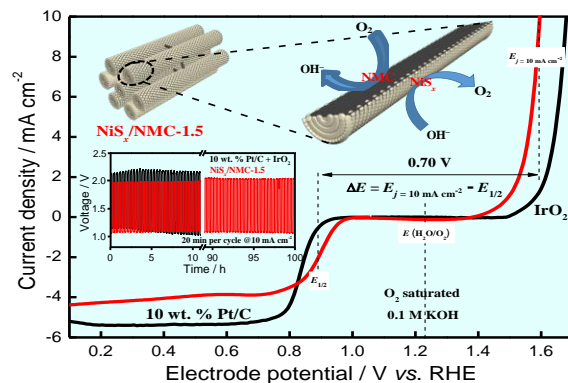
Corresponding Author

*E-mail: jiangshui.luo@kuleuven.be (J. Luo), *E-mail: xuan.zhang@kuleuven.be (X. Zhang),

*E-mail: jan.fransaer@kuleuven.be (J. Fransaer).

ABSTRACT: A highly ordered mesoporous nickel sulfides/nitrogen-doped mesoporous carbon (NiS_x/NMC , NiS_x : NiS and Ni_3S_4) nano hybrid was synthesized by the assistant of NMC template. Using of NMC as a template, improves the electronic conductivity of the catalyst, while the high specific surface area increases the number of active sites and the highly ordered mesoporous structure enables fast mass transfer. As a result, the resultant NiS_x/NMC is one of the most active bifunctional oxygen electrocatalysts with a low potential gap of 0.70 V. The primary Zn-air battery shows a maximum power density of 186 mW cm^{-2} and an energy density as high as 805 Wh kg^{-1} at 100 mA cm^{-2} . The battery also exhibits favorable long-term cycling behaviour (the polarization increased only 0.05 V after 300 charge/discharge cycles for 100 h). This work provides a new strategy for the rational design of metal-carbon nano hybrid electrocatalysts for low-cost energy storage and conversion devices.

TOC GRAPHICS



Rechargeable Zn-air batteries are interesting energy storage systems due to their high theoretical energy density (1086 Wh kg^{-1}), environmental friendliness and safety.¹⁻⁴ The oxygen reduction reaction (ORR) and oxygen evolution reaction (OER) are the key electrochemical reactions for the discharge and charge processes of the Zn-air batteries, respectively. However, these two reactions exhibit sluggish kinetics due to the four-electron transfer process, and require noble metals as catalysts to construct efficient energy storage devices.⁵⁻⁸ Currently, Pt-based catalysts are considered as the most efficient ORR catalysts,⁹⁻¹⁰ and IrO₂ and RuO₂ are regarded as the most efficient OER catalysts.¹¹⁻¹² However, the scarcity and concomitant high cost of Ru and Ir severely hamper their application for Zn-air batteries.¹³⁻¹⁵ Therefore, a lot of efforts have been devoted to finding alternative bifunctional electrocatalysts with low-cost, high activity and stability.¹⁶⁻¹⁹

In the past years, nitrogen-doped carbons with high specific surface area and modified electronic structure have achieved outstanding electrocatalytic activity for ORR in aqueous alkaline solutions.²⁰⁻²³ On the other hand, transition metal-based materials have been considered as promising electrocatalysts for OER due to their low cost and high activity.²⁴⁻²⁶ Therefore, transition metal-based materials coupled to nitrogen-doped carbon is an effective strategy for the preparation of nanohybrids as bifunctional oxygen electrocatalysts. For instance, Hu *et al.* developed NiCo₂S₄ nanocrystals anchored on nitrogen-doped carbon nanotubes (NiCo₂S₄/N-CNT) as a bifunctional catalyst.²⁷ The catalyst displayed excellent electrocatalytic activity towards ORR ($E_{1/2} = 0.80 \text{ V}$) and OER ($\eta = 0.37 \text{ V}$ at 10 mA cm^{-2}). A Zn-air battery using this catalyst showed a peak power density of 147 mW cm^{-2} and had an energy density of 555 Wh kg^{-1} , respectively. The polarization increased 0.06 V after 150 charge-discharge cycles at 10 mA cm^{-2} . Chen *et al.* fabricated a hierarchical porous double-shelled (Mg, Co)₃O₄ encapsulated in N-doped graphitized carbon, where the Mg substitution facilitates the mass transport and also improves electrical conductivity.¹⁷

The catalyst exhibited a high electrocatalytic activity towards ORR ($E_{1/2} = 0.842$ V) and OER ($\eta = 0.346$ V at 10 mA cm^{-2}). The rechargeable Zn-air battery using this catalyst displayed a peak power density of 125 mW cm^{-2} and a long-term cyclability at 10 mA cm^{-2} (2 h per cycle for 100 cycles).¹⁷ Goodenough *et al.* reported Ni₃Fe nanoparticles embedded in porous nitrogen-doped carbon sheets (Ni₃Fe/N-C sheets) by a pyrolysis-based route using NaCl crystals as a template. The obtained Ni₃Fe/N-C sheets showed good electrocatalytic activity towards ORR ($E_{1/2} = 0.78$ V) and OER ($\eta = 0.37$ V at 10 mA cm^{-2}). The corresponding Zn-air battery showed good cycling stability at 10 mA cm^{-2} for 105 cycles with an energy density of 634 Wh kg^{-1} .²⁸ Despite the significant progress, the electrocatalytic performance and cycling stability of the reported nanohybrids are not yet satisfactory for the practical applications of Zn-air batteries. Clearly, the development of alternative air-cathode electrocatalysts with low cost, high performance, and superior cycling stability for Zn-air batteries is highly challenging and hence research in this direction is needed to obtain efficient catalytic materials for application in air cathodes.

Here, we conducted the template-directed synthesis of highly ordered mesoporous nickel sulfides/nitrogen-doped mesoporous carbon (NiS_x/NMC) nanohybrids as an advanced oxygen electrocatalyst for Zn-air batteries. The NiS_x follows the ordered mesoporous structure of the NMC template and is uniformly attached on the surface of NMC. Owing to the combined effect of nitrogen-doped carbon and nickel sulfide in the nanohybrid structure, the optimized NiS_x/NMC catalyst exhibits outstanding electrocatalytic activity with a small potential gap (ΔE) of 0.70 V. On the one hand, the NMC was highly active to ORR and nickel sulfides was highly active to OER. On the other hand, using the NMC template improves the electronic conductivity of the catalyst, while the high specific surface area increases the number of accessible active sites and the highly ordered mesoporous structure promotes the efficient mass transfer of reactants. The

primary Zn-air battery using this electrocatalyst achieved a maximum power density of 186 mW cm⁻², and an energy density of 805 Wh kg⁻¹, as well as long-term cycling durability of 300 charge/discharge cycles for 100 h.

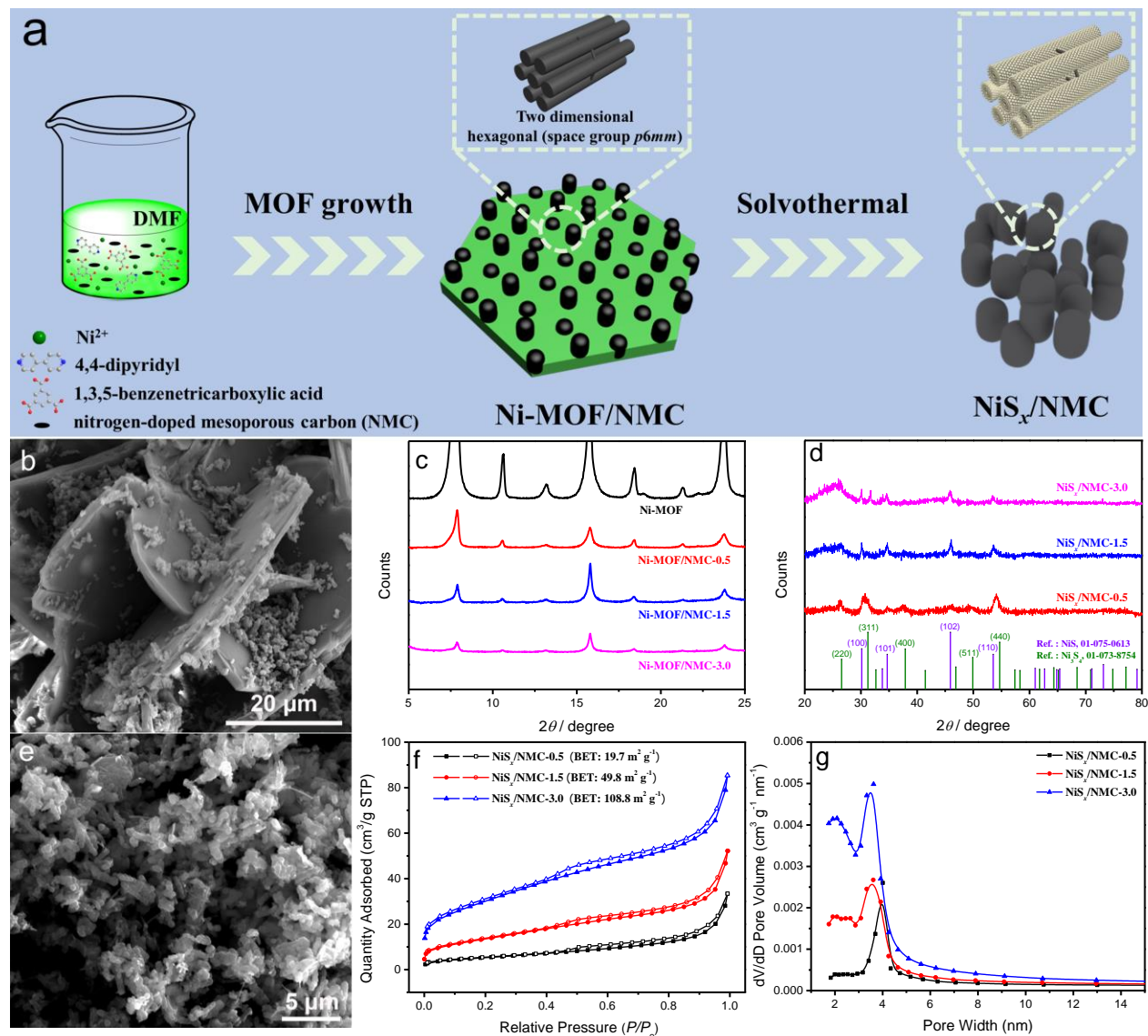


Figure 1. (a) Schematic illustration of the synthesis of NiS_x/NMC nanohybrids, (b) SEM image of the Ni-MOF/NMC-1.5, (c) XRD patterns of the Ni-MOF/NMC samples, (d) XRD patterns of the obtained NiS_x/NMC nanohybrids, (e) SEM image of NiS_x/NMC-1.5, (f) Nitrogen

adsorption/desorption isotherms of the NiS_x/NMC nanohybrids and (g) the corresponding pore volume distribution.

The schematic diagram of the synthesis process of NiS_x/NMC nanohybrid is shown in **Figure 1a**. Firstly, the Ni-MOF/NMC nanocomposites were synthesized by dissolving nickel(II) nitrate hexahydrate ($\text{Ni}(\text{NO}_3)_2 \cdot 6\text{H}_2\text{O}$) and organic linkers in DMF in the presence of NMC particles at 50 °C for 72 h. Scanning electron microscopy (SEM) images show that the NMC particles are distributed both on the surface and inside of Ni-MOF blocks (**Figure 1b** and **Figure S1**). The Ni-MOFs were almost fully covered by the NMC particles when increasing the concentration of NMC from 0.5 mg mL⁻¹ to 3.0 mg mL⁻¹ (**Figure S1d**). The Ni-MOF/NMC nanocomposites exhibit the same diffraction peaks as the Ni-MOF,²⁹ indicating the successful synthesis of Ni-MOFs in the presence of NMC particles (**Figure 1c** and **Figure S2**). Subsequently, the Ni-MOF/NMC nanocomposites were subjected to a solvothermal process at 150 °C in ethanol in the presences of Na_2S , where the NMC served as a template. The X-ray diffraction results confirmed that there are two kinds of nickel sulfides (NiS and Ni_3S_4) in the obtained nanohybrid (**Figure 1d**). The 2θ diffraction peaks at 30.1°, 34.7°, 45.9°, and 53.5° correspond to the (100), (101), (102), and (110) planes of hexagonal NiS (JCPDS: 01-075-0613), respectively. The 2θ diffraction peaks at 26.6°, 31.2°, 37.9°, 49.9°, and 54.7° correspond to the (220), (311), (400), (511), and (440) planes of cubic Ni_3S_4 (JCPDS: 01-073-8754), respectively.³⁰ Furthermore, the SEM images reveal that the Ni-MOF structure was destroyed and only the NMC particles remained after solvothermal treatment (**Figure 1e** and **Figure S3**). N_2 adsorption/desorption isotherm and pore size distribution plots were used to investigate the porous structure of the NiS_x , NMC, and NiS_x/NMC nanohybrid (**Figure 1f**, **Figure 1g** and **Figure S4**). All of the NiS_x/NMC nanohybrids exhibit typical type-IV isotherms with an H1 hysteresis loop, confirming their ordered mesoporous structure.^{8, 31} When

the NMC concentration increased from 0.5 mg mL^{-1} to 3.0 mg mL^{-1} , the specific surface area of the nanohybrids increases from $20 \text{ m}^2 \text{ g}^{-1}$ to $110 \text{ m}^2 \text{ g}^{-1}$, owing to the high specific surface area of NMC ($746 \text{ m}^2 \text{ g}^{-1}$). The pore diameters of the NiS_x/NMC nanohybrids (ranging from 3.5 nm to 4.0 nm) are larger than NMC (3.0 nm, **Figure S5b**), which may be ascribed to the large pore of NiS_x on the pore walls of the NMC.

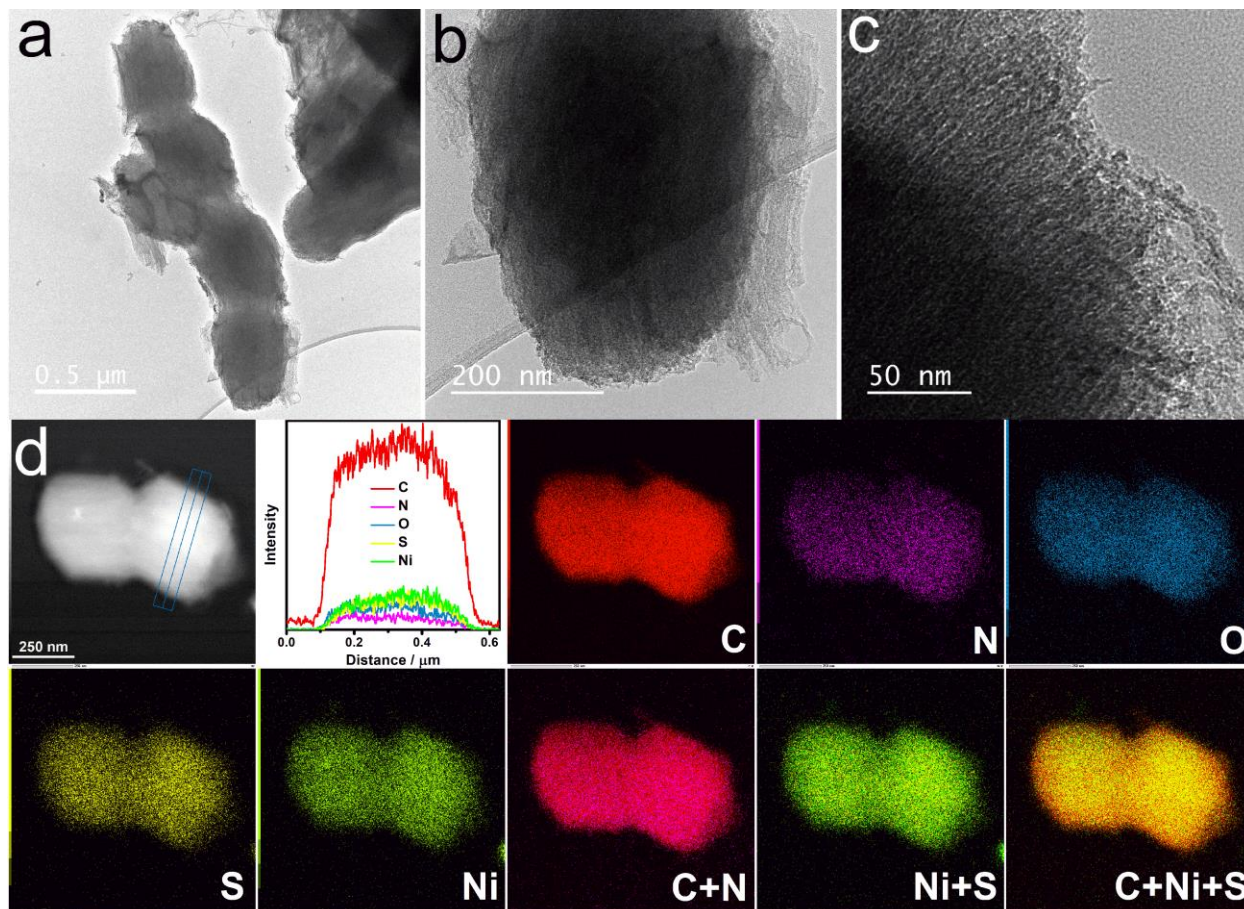


Figure 2. TEM images at a resolution of (a) $0.5 \mu\text{m}$, (b) 200 nm , and (c) 50 nm ; (d) EDS line scan and maps of $\text{NiS}_x/\text{NMC-1.5}$.

Transmission electron microscopy (TEM) images show that the $\text{NiS}_x/\text{NMC-1.5}$ nanohybrid exhibits necklace-like connected spherical particles with a highly ordered mesoporous structure, which perfectly copies the template structure of NMC (**Figure 2**). The line scan results show that the element of C exhibits much higher intensity than the other elements. This result suggests that

the N, O, S, and Ni elements are distributed on the surface of the NMC particles. The elemental mapping results confirm the uniform distribution of C, N, O, S, and Ni. These results indicate that NiS_x was attached to the highly ordered mesoporous NMC template. The $\text{NiS}_x/\text{NMC}-3.0$ nanohybrids show similar morphology and elemental distribution (Figure S6d-f). For the sample of $\text{NiS}_x/\text{NMC}-0.5$, the majority of nickel sulfides was uniformly distributed on the structure of NMC, however, it was also partially agglomerated and connected to the NMC particles, which may be attributed to the excess nickel sulfides when a low NMC concentration (0.5 mg mL^{-1}) was used (Figure S6a-c). The inductively coupled plasma optical emission spectroscopy (ICP-OES) confirmed that the Ni contents follow the order: decreased from 14.9 wt. % for $\text{NiS}_x/\text{NMC}-0.5 > 8.4 \text{ wt. \%}$ for $\text{NiS}_x/\text{NMC}-1.5 > 4.8 \text{ wt. \%}$ for $\text{NiS}_x/\text{NMC}-3.0$, when increasing the NMC concentration from 0.5 mg mL^{-1} to 3.0 mg mL^{-1} (Figure S7).

X-ray photoelectron spectroscopy (XPS) was employed to detect the surface elemental compositions and chemical states of the NiS_x/NMC nanohybrids. Clearly, C, N, O, S, and Ni were detected on the surface of NiS_x/NMC nanohybrids (Figure S8 and Table S1). The Ni content decreased rapidly as the concentration of NMC increased from 0.5 mg mL^{-1} to 3.0 mg mL^{-1} (Figure 3a), which is consistent with the ICP-OES results. In order to get further insight into the chemical states, the N 1s, S 2p, and Ni 2p spectra of the nanohybrids were deconvoluted (Figure 3b-d). The N 1s peaks at 398.65 eV, 399.72 eV, 401.28 eV, and 403.20 eV correspond to pyridinic-N, pyrrolic-N, graphitic-N, and N-O, respectively.³²⁻³³ The nitrogen-activated carbon has been considered as the active sites of ORR, which exhibits a positive charge density thus facilitates the adsorption of the oxygen during ORR.²⁰⁻²¹ The peaks at 162.39 eV, 163.74 eV, and 165.01 eV were attributed to the S 2p_{3/2} of S^{2-} , S 2p_{1/2} of S^{2-} , and the bridging S_2^{2-} , respectively.³⁴⁻³⁶ The Ni 2p peaks at 857.53 eV, 875.51 eV, and 862.61/881.17 eV were assigned to the Ni 2p_{3/2}, Ni 2p_{1/2},

and satellite peaks, respectively. The Ni 2p_{3/2} peak was deconvoluted into two peaks of Ni²⁺ and Ni³⁺. The peak area of the Ni³⁺ was much larger than that of Ni²⁺, indicating the high content of high-valence Ni³⁺. It is proposed that the surface of the electrocatalyst was slightly oxidized to Ni³⁺ under OER conditions.³⁷⁻⁴⁰ The high-valence Ni³⁺ enhanced the chemisorption of OH⁻ on its surface and favors the formation of NiOOH, which facilitates the electron transfer to the surface during OER.⁴¹ Therefore, the obtained NiS_x/NMC catalysts were expected to display a superior activity toward ORR and OER.

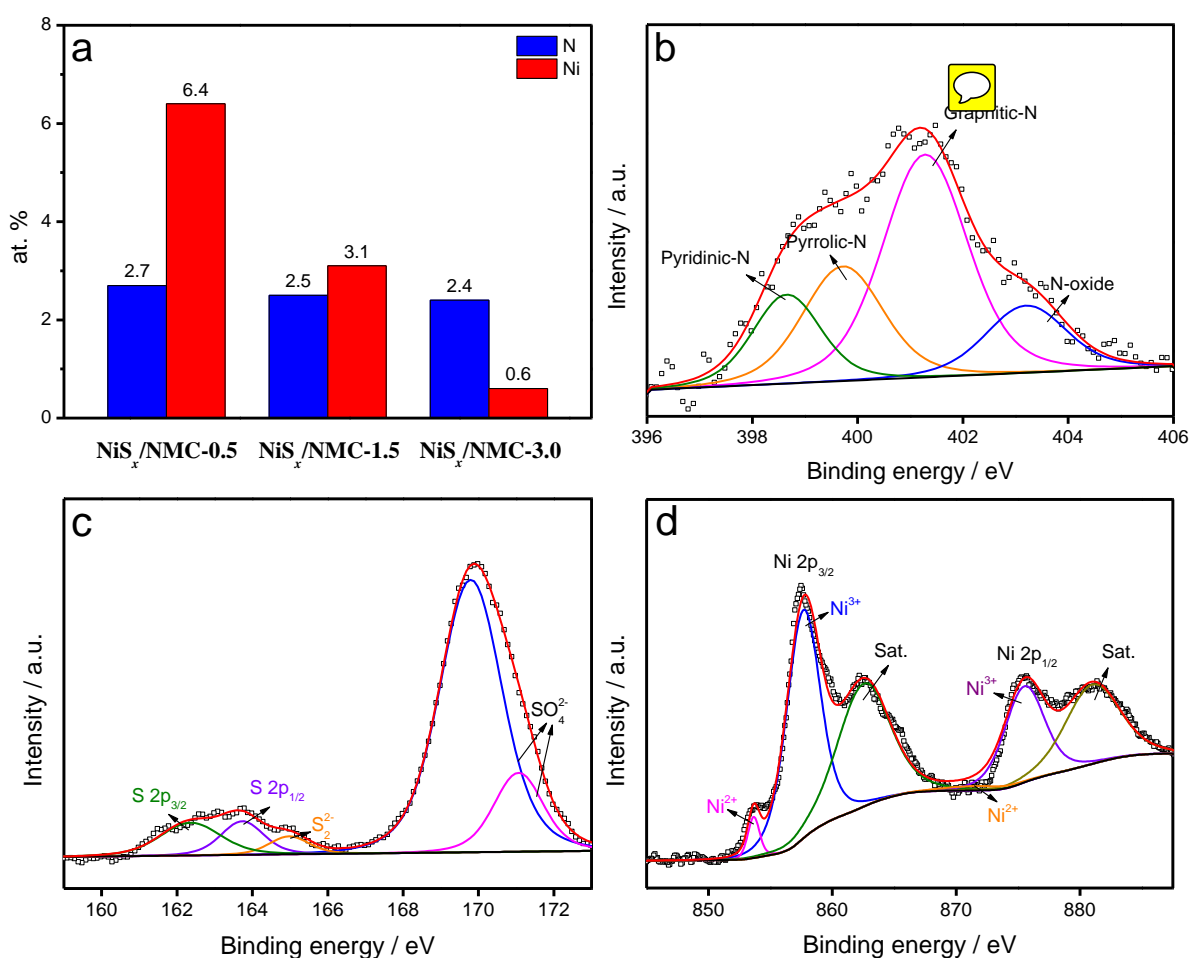


Figure 3. (a) Surface elemental content of nitrogen and nickel of the NiS_x/NMC nanohybrids as determined by XPS; (b) N 1s peak and peak fitting results of NiS_x/NMC-0.5; (c) S 2p peak and peak fitting results of NiS_x/NMC-0.5; (d) Ni 2p peaks and peak fitting results of NiS_x/NMC-0.5.

The electrocatalytic performances of the as-prepared catalysts for the ORR and OER were evaluated in 0.1 M KOH solution (Figure 4 and Figure S9). In terms of ORR performances, the NiS_x/NMC catalysts exhibit a significant enhancement of ORR activity after the introduction of NMC (Figure 4a). Among them, the NiS_x/NMC-1.5, NiS_x/NMC-3.0, and NMC exhibit better ORR activities than that of commercial 10 wt. % Pt/C. The half-wave potentials ($E_{1/2}$) of the catalysts were observed to decrease in the following order: 0.898 V for NiS_x/NMC-3.0, 0.893 V for NMC, 0.890 V for NiS_x/NMC-1.5, 0.837 V for 10 wt. % Pt/C, and 0.801 V for NiS_x/NMC-0.5 (Figure S10). For the NiS_x/NMC nanohybrids, the ORR activities were observed to increase with the increasing NMC concentration from 0.5 mg mL⁻¹ to 3.0 mg mL⁻¹, which may be attributed to the increased active NMC in the materials. However, the NiS_x/NMC-3.0 exhibits a higher onset potential than NMC, which may be attributed to the synergistic effects between the highly dispersed NiS_x and NMC. Furthermore, the electron transfer number of the as-synthesized nanohybrids was calculated based on the Koutecky-Levich equation (K-L) (Figure 4b and Figure S11). Clearly, NiS_x/NMC-1.5, NiS_x/NMC-3.0, and NMC show high selectivity and favor the four electron reduction of oxygen with an electron transfer number of around 3.9.

For the OER process, the NiS_x displayed the highest OER activity than the other catalysts, while the NMC exhibited a negligible OER activity (Figure 4c). The OER activity decreased with the increasing concentration of NMC. The NiS_x/NMC-0.5 and NiS_x/NMC-1.5 both exhibit an overpotential (η) around 0.36 V, which is lower than that of NiS_x/NMC-3.0 (0.394 V) and IrO₂ (0.453 V) at a current density of 10 mA cm⁻² (Figure S12). Charge transfer resistance (R_{ct}) of the OER was evaluated by electrochemical impedance spectroscopy (Figure 4d). The NiS_x/NMC nanohybrids exhibited a lower charge transfer resistance than the non-template NiS_x, indicating the improved electronic conductivity in the presence of NMC. The NiS_x/NMC-3.0 shows a larger

charge transfer resistance (27.7 Ω) than that of NiS_x/NMC-0.5 (15.2 Ω) and NiS_x/NMC-1.5 (16.4

Ω).

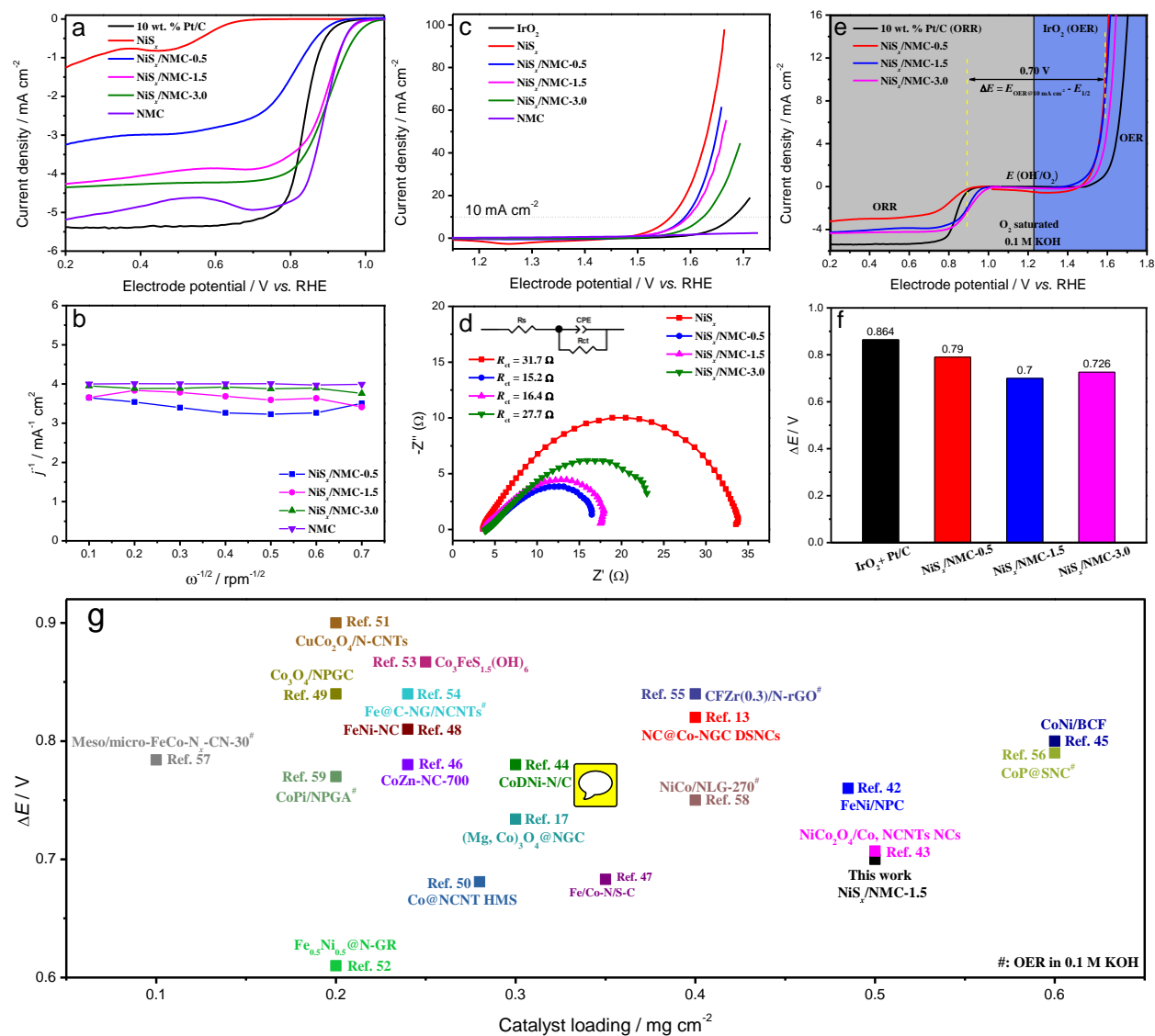



Figure 4. (a) The ORR polarization curves in 0.1 M O₂-saturated KOH at 1600 rpm. (b) The electron transfer number of the catalysts. (c) The OER polarization curves the catalysts in 0.1 M O₂-saturated KOH at 1600 rpm. (d) Nyquist plots and fitting results of the catalysts in the frequency range from 100 kHz to 0.1 Hz with an amplitude of 5 mV at 1.61 V vs. RHE; Inset is the equivalent circuit, where R_s is the resistance of the electrolyte, R_{ct} is the charge transfer resistance, and CPE is a constant phase element. (e) ORR and OER polarization curves of

NiS_x/NMC nanohybrids, 10 wt. % Pt/C (for ORR), and IrO₂ (for OER). (f) The ΔE value between $E_{j=10}$ and $E_{1/2}$ of the catalysts. (g) Comparison of ΔE value of NiS_x/NMC-1.5 with previously reported bifunctional catalysts.^{13, 17, 42-59}

For a bifunctional electrocatalyst, the reversible oxygen activity is usually evaluated by the potential gap ($\Delta E = E_{j=10} - E_{1/2}$) between $E_{j=10}$ (potential of OER at 10 mA cm⁻²) and $E_{1/2}$ of ORR (**Figure 4e**). The smaller the value of ΔE , the more active and reversible the oxygen electrode is. The ΔE value of NiS_x/NMC-1.5 is 0.70 V, which is lower than 0.864 V for the 10 wt. % Pt/C+IrO₂ hybrid (**Figure 4f**). This makes the NiS_x/NMC-1.5 nanohybrid one of the best bifunctional catalysts reported  the literature (**Figure 4g**). The superior bifunctional electrocatalytic performance was attributed to the following factors. First, the highly ordered mesoporous NiS_x/NMC nanohybrid exhibits highly electrocatalytic activity towards both ORR and OER. Second, the nickel sulfides are uniformly attached on the surface of the NMC, which is beneficial for the electronic conductivity of the catalyst. Third, the high specific surface area results in a high number of active sites while the ordered mesoporous structure favours the mass transfer of reactants.

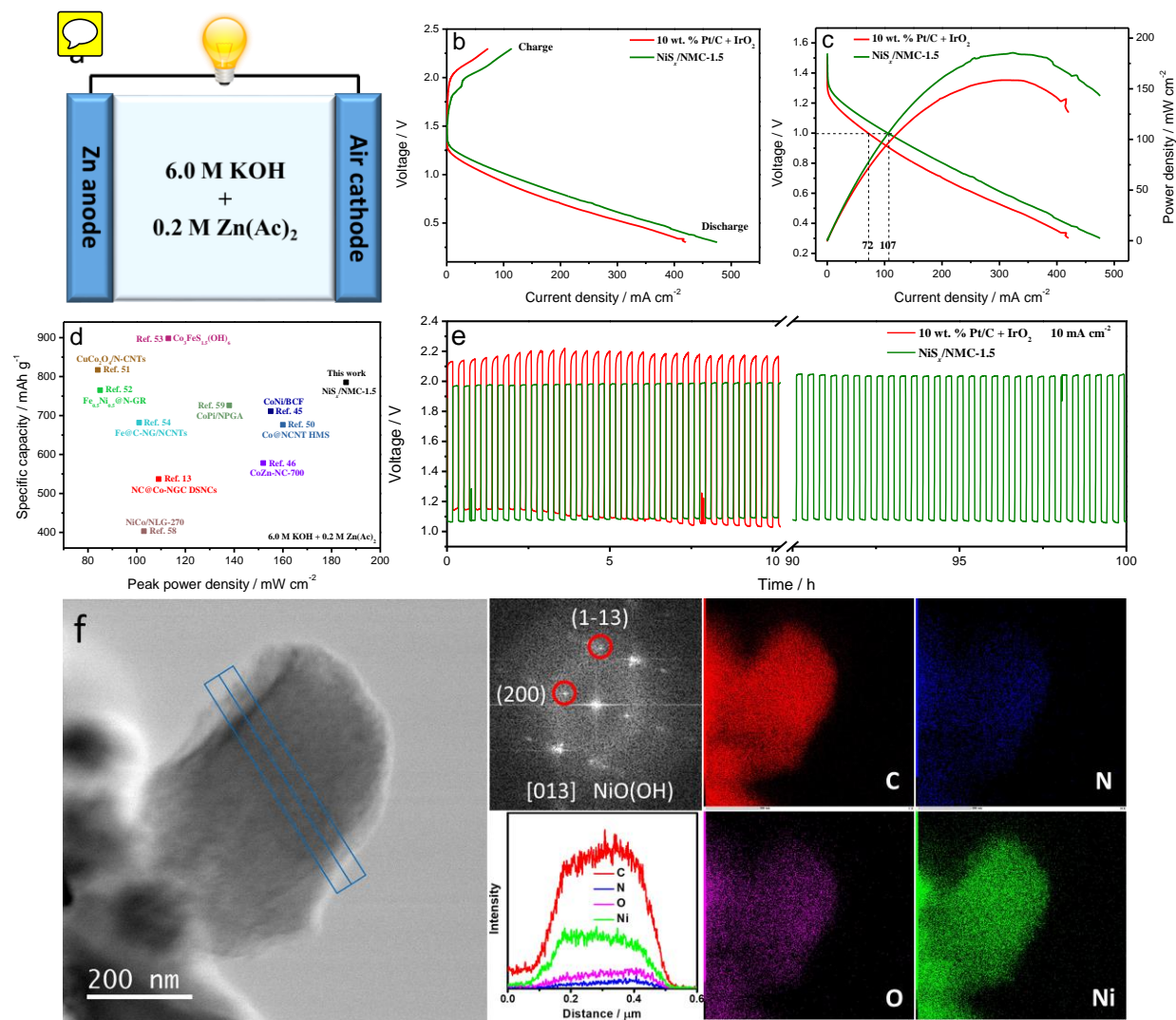


Figure 5. (a) Schematic illustration of a rechargeable Zn-air battery. (b) Charge and discharge polarization curves of $\text{NiS}_x/\text{NMC-1.5}$ electrode and 10 wt. % Pt/C + IrO_2 hybrid electrode. (c) The corresponding polarization curves and power density curves. (d) Comparison of peak power density and specific capacity of the Zn-air batteries with $\text{NiS}_x/\text{NMC-1.5}$ and previously reported bifunctional catalysts.^{13, 45-46, 50-54, 58-59} (e) Charge-discharge cycling stability of the Zn-air batteries with a $\text{NiS}_x/\text{NMC-1.5}$ electrode vs. a 10 wt. % Pt/C + IrO_2 hybrid electrode at 10 mA cm^{-2} . (f) TEM image, EDS line scan, and maps of the $\text{NiS}_x/\text{NMC-1.5}$ air cathode after long-term cycling.



Finally, the $\text{NiS}_x/\text{NMC}-1.5$ nanohybrid was used as an air electrode in rechargeable Zn-air batteries (**Figure 5a** and **Figure S13**). The open circuit voltage (OCV) of the Zn-air battery is 1.53 V (**Figure S14**). It shows lower charge and discharge overpotential at various current densities than that of the 10 wt. % Pt/C+IrO₂ hybrid electrode. In particular, a peak power density of 186 mW cm⁻² at a current density of 323 mA cm⁻² was achieved for the $\text{NiS}_x/\text{NMC}-1.5$ electrode (**Figure 5c**), which makes it one of the best-performing air electrodes (**Figure 5d** and **Table S2**). Moreover, at a cell voltage of 1.0 V, the $\text{NiS}_x/\text{NMC}-1.5$ electrode shows a current density of 107 mA cm⁻², which is significantly higher than the 72 mA cm⁻² obtained for the 10 wt. % Pt/C+IrO₂ hybrid electrode. The specific capacity and energy density were calculated to be 785 mAh g⁻¹ and 805 Wh kg⁻¹ at a discharge current density of 100 mA cm⁻², respectively (**Figure S15**). The charge-discharge cycling stability was further investigated by galvanostatic technique at 10 mA cm⁻² (**Figure 5e**). The discharge voltage plateau is found to be around 1.08 V and exhibits negligible decrease even after 300 cycles (20 min per cycle for a total time of 100 h). Only a small increase from 1.98 V to 2.03 V was observed for the charge voltage plateau after continuous cycling for 100 h. In contrast, the discharge voltage plateau of the Zn-air battery using the 10 wt. % Pt/C+IrO₂ hybrid electrode decreased rapidly after cycling for 10 h. The TEM image, EDS line scan, and maps of the post-cycling product is shown in **Figure 5f**. It is found that the NMC as remained its morphology of spherical particle, while the S element was lost from the NiS_x. The EDS line scan and maps show that the N and Ni element still uniformly distributed on the surface of NMC. The OER activated species of NiOOH was detected from the post-cycling product, which generated under oxidation conditions during the charging process. This results suggested that the long-term durability is assigned to the stabled $\text{NiS}_x/\text{NMC}-1.5$ structure and active species of

ORR and OER. The outstanding cycling stability makes the NiS_x/NMC-1.5 nanohybrid a promising catalyst for the air electrode in practical Zn-air batteries.

In summary, a highly ordered mesoporous nickel sulfides/nitrogen-doped mesoporous carbon (NiS_x/NMC) nanohybrid was synthesized through a template-assisted method as bifunctional oxygen electrocatalyst for rechargeable Zn-air batteries. The optimized NiS_x/NMC nanohybrid (denoted as NiS_x/NMC-1.5) shows high ORR and OER electrocatalytic activities with a small potential gap (ΔE) of 0.70 V. The outstanding electrocatalytic activity was attributed to the uniform distribution of highly active species and improved electronic conductivity of the NiS_x/NMC nanohybrid. Additionally, the high specific surface area increases the number of accessible active sites while the unique ordered mesoporous structure enables fast mass transfer of reactant species. A primary Zn-air battery with the NiS_x/NMC-1.5 nanohybrid as the catalyst for the air-electrode exhibited a maximum power density of 186 mW cm⁻² and an energy density of 805 Wh kg⁻¹, as well as excellent durability after 300 charge/discharge cycles for 100 h. This work provides a new strategy for the rational design of metal-carbon nanohybrid electrocatalysts for low-cost energy storage and conversion devices like rechargeable batteries and unitized regenerative fuel cells.

ASSOCIATED CONTENT

Supporting Information.

Experimental Section; Figures S1–S15 and Tables S1–S2 as described in the text (PDF)

AUTHOR INFORMATION

Corresponding Authors

*E-mail: jiangshui.luo@kuleuven.be (J. Luo).

*E-mail: jan.fransaer@kuleuven.be (J. Fransaer).

ORCID

Kai Wan: 0000-0003-4689-310X

Chen Zhou: 0000-0002-4619-9014

Jin Won Seo: 0000-0003-4937-0769

Palaniappan Subramanian: 0000-0003-1000-6994

Jia-wei Yan: 0000-0002-0045-6169

Notes

The authors declare no competing financial interest.

ACKNOWLEDGMENT

K. Wan is grateful to the Oversea Study Program of Guangzhou Elite Project. X. Zhang is grateful to the China Scholarship Council. J. Luo acknowledges the Research Foundation – Flanders (FWO) for a Research Project (G0B3218N) and a Research Grant (1529816N). Funding from the National Natural Science Foundation of China (No. 21776120), and “Minjiang Scholar” Program and key project (No. JZ160480) of Department of Education, Fujian Province, China is acknowledged. The Open Project Program of Provincial Key Laboratory of Clean Energy Materials, Longyan University (QJNY-201705) is also acknowledged.

REFERENCES

- (1) Wang, H. F.; Tang, C.; Zhang, Q. A review of precious-metal-free bifunctional oxygen electrocatalysts: Rational design and applications in Zn–air batteries. *Adv. Funct. Mater.* **2018**, *28*, 1803329.
- (2) Pan, J.; Xu, Y. Y.; Yang, H.; Dong, Z.; Liu, H.; Xia, B. Y. Advanced architectures and relatives of air electrodes in Zn–air batteries. *Adv. Sci.* **2018**, *5*, 1700691.
- (3) Li, Y.; Dai, H. Recent advances in zinc–air batteries. *Chem. Soc. Rev.* **2014**, *43*, 5257-5275.

(4) Li, Y.; Lu, J. Metal–air batteries: Will they be the future electrochemical energy storage device of choice? *ACS Energy Lett.* **2017**, *2*, 1370-1377.

(5) Zhang, X.; Luo, J.; Lin, H. F.; Tang, P.; Morante, J. R.; Arbiol, J.; Wan, K.; Mao, B. W.; Liu, L. M.; Fransaer, J. Tailor-made metal-nitrogen-carbon bifunctional electrocatalysts for rechargeable Zn–air batteries via controllable MOF units. *Energy Storage Mater.* **2019**, *17*, 46-61.

(6) Wan, K.; Yu, Z. P.; Li, X. H.; Liu, M. Y.; Yang, G.; Piao, J. H.; Liang, Z. X. pH effect on electrochemistry of nitrogen-doped carbon catalyst for oxygen reduction reaction. *ACS Catal.* **2015**, *5*, 4325-4332.

(7) Zhang, X.; Luo, J.; Wan, K.; Plessers, D.; Sels, B.; Song, J.; Chen, L.; Zhang, T.; Tang, P.; Morante, J. R.; Arbiol, J.; Fransaer, J. From rational design of a new bimetallic MOF family with tunable linkers to oer catalysts. *J. Mater. Chem. A* **2019**, *7*, 1616-1628.

(8) Wan, K.; Long, G. F.; Liu, M. Y.; Du, L.; Liang, Z. X.; Tsiakaras, P. Nitrogen-doped ordered mesoporous carbon: Synthesis and active sites for electrocatalysis of oxygen reduction reaction. *Appl. Catal. B Environ.* **2015**, *165*, 566-571.

(9) Zhang, B. W.; Zhang, Z. C.; Liao, H. G.; Gong, Y.; Gu, L.; Qu, X. M.; You, L. X.; Liu, S.; Huang, L.; Tian, X. C.; Huang, R.; Zhu, F. C.; Liu, T.; Jiang, Y. X.; Zhou, Z. Y.; Sun, S. G. Tuning Pt-skin to Ni-rich surface of Pt₃Ni catalysts supported on porous carbon for enhanced oxygen reduction reaction and formic electro-oxidation. *Nano Energy* **2016**, *19*, 198-209.

(10) Chong, L.; Wen, J.; Kubal, J.; Sen, F. G.; Zou, J.; Greeley, J.; Chan, M.; Barkholtz, H.; Ding, W.; Liu, D. J. Ultralow-loading platinum-cobalt fuel cell catalysts derived from imidazolate frameworks. *Science* **2018**, *362*, 1276-1281.

(11) Rao, R. R.; Kolb, M. J.; Halck, N. B.; Pedersen, A. F.; Mehta, A.; You, H.; Stoerzinger, K. A.; Feng, Z.; Hansen, H. A.; Zhou, H.; Giordano, L.; Rossmeisl, J.; Vegge, T.; Chorkendorff, I.

Stephens, I. E. L.; Shao-Horn, Y. Towards identifying the active sites on RuO₂(110) in catalyzing oxygen evolution. *Energ. Environ. Sci.* **2017**, *10*, 2626-2637.

(12) Kuo, D. Y.; Kawasaki, J. K.; Nelson, J. N.; Kloppenburg, J.; Hautier, G.; Shen, K. M.; Schlom, D. G.; Suntivich, J. Influence of surface adsorption on the oxygen evolution reaction on IrO₂(110). *J. Am. Chem. Soc.* **2017**, *139*, 3473-3479.

(13) Liu, S.; Wang, Z.; Zhou, S.; Yu, F.; Yu, M.; Chiang, C. Y.; Zhou, W.; Zhao, J.; Qiu, J. Metal-organic-framework-derived hybrid carbon nanocages as a bifunctional electrocatalyst for oxygen reduction and evolution. *Adv. Mater.* **2017**, *29*, 1700874.

(14) Niu, W.; Li, Z.; Marcus, K.; Zhou, L.; Li, Y.; Ye, R.; Liang, K.; Yang, Y. Surface-modified porous carbon nitride composites as highly efficient electrocatalyst for Zn-air batteries. *Adv. Energy Mater.* **2018**, *8*, 1701642.

(15) Lai, Q.; Zhu, J.; Zhao, Y.; Liang, Y.; He, J.; Chen, J. MOF-based metal-doping-induced synthesis of hierarchical porous Cu@N/C oxygen reduction electrocatalysts for Zn-air batteries. *Small* **2017**, *13*, 1700740.

(16) Zhu, J.; Xiao, M.; Zhang, Y.; Jin, Z.; Peng, Z.; Liu, C.; Chen, S.; Ge, J.; Xing, W. Metal-organic framework-induced synthesis of ultrasmall encased NiFe nanoparticles coupling with graphene as an efficient oxygen electrode for a rechargeable Zn-air battery. *ACS Catal.* **2016**, *6*, 6335-6342.

(17) Deng, Y. P.; Jiang, Y.; Luo, D.; Fu, J.; Liang, R.; Cheng, S.; Bai, Z.; Liu, Y.; Lei, W.; Yang, L.; Jing, Z.; Zhongwei, C. Hierarchical porous double-shelled electrocatalyst with tailored lattice alkalinity toward bifunctional oxygen reactions for metal-air batteries. *ACS Energy Lett.* **2017**, *2*, 2706-2712.

- (18) Huang, X.; Zhang, Y.; Shen, H.; Li, W.; Shen, T.; Ali, Z.; Tang, T.; Guo, S.; Sun, Q.; Hou, Y. N-doped carbon nanosheet networks with favorable active sites triggered by metal nanoparticles as bifunctional oxygen electrocatalysts. *ACS Energy Lett.* **2018**, *3*, 2914-2920.
- (19) Zhu, L.; Zheng, D.; Wang, Z.; Zheng, X.; Fang, P.; Zhu, J.; Yu, M.; Tong, Y.; Lu, X. A confinement strategy for stabilizing ZIF-derived bifunctional catalysts as a benchmark cathode of flexible all-solid-state zinc–air batteries. *Adv. Mater.* **2018**, *30*, 1805268.
- (20) Gong, K.; Du, F.; Xia, Z.; Durstock, M.; Dai, L. Nitrogen-doped carbon nanotube arrays with high electrocatalytic activity for oxygen reduction. *Science* **2009**, *323*, 760-764.
- (21) Guo, D. H.; Shibuya, R.; Akiba, C.; Saji, S.; Kondo, T.; Nakamura, J. Active sites of nitrogen-doped carbon materials for oxygen reduction reaction clarified using model catalysts. *Science* **2016**, *351*, 361-365.
- (22) Liang, H. W.; Zhuang, X.; Bruller, S.; Feng, X.; Mullen, K. Hierarchically porous carbons with optimized nitrogen doping as highly active electrocatalysts for oxygen reduction. *Nat. Commun.* **2014**, *5*, 4973.
- (23) Li, Y.; Zhou, W.; Wang, H.; Xie, L.; Liang, Y.; Wei, F.; Idrobo, J. C.; Pennycook, S. J.; Dai, H. An oxygen reduction electrocatalyst based on carbon nanotube-graphene complexes. *Nat. Nanotechnol.* **2012**, *7*, 394-400.
- (24) Kim, J. S.; Kim, B.; Kim, H.; Kang, K. Recent progress on multimetal oxide catalysts for the oxygen evolution reaction. *Adv. Energy Mater.* **2018**, *8*, 1702774.
- (25) Vij, V.; Sultan, S.; Harzandi, A. M.; Meena, A.; Tiwari, J. N.; Lee, W. G.; Yoon, T.; Kim, K. S. Nickel-based electrocatalysts for energy-related applications: Oxygen reduction, oxygen evolution, and hydrogen evolution reactions. *ACS Catal.* **2017**, *7*, 7196-7225.

- (26) Suen, N. T.; Hung, S. F.; Quan, Q.; Zhang, N.; Xu, Y. J.; Chen, H. M. Electrocatalysis for the oxygen evolution reaction: Recent development and future perspectives. *Chem. Soc. Rev.* **2017**, *46*, 337-365.
- (27) Han, X. P.; Wu, X. Y.; Zhong, C.; Deng, Y. D.; Zhao, N. Q.; Hu, W. B. NiCo₂S₄ nanocrystals anchored on nitrogen-doped carbon nanotubes as a highly efficient bifunctional electrocatalyst for rechargeable zinc–air batteries. *Nano Energy* **2017**, *31*, 541-550.
- (28) Fu, G.; Cui, Z.; Chen, Y.; Li, Y.; Tang, Y.; Goodenough, J. B. Ni₃Fe-N doped carbon sheets as a bifunctional electrocatalyst for air cathodes. *Adv. Energy Mater.* **2017**, *7*, 1601172.
- (29) Li, Y.; Xie, L.; Liu, Y.; Yang, R.; Li, X. Favorable hydrogen storage properties of M(HBTC)(4,4'-bipy)·3DMF (M = Ni and Co). *Inorg. Chem.* **2008**, *47*, 10372-10377.
- (30) Pan, W.; Huang, Y.; Cui, S.; Chen, W.; Mi, L. Fabrication of CuS@Ni₃S₄-polyacrylonitrile textile fabric with enhanced reusability for the treatment of dyes wastewater. *ChemistrySelect* **2016**, *1*, 3618-3622.
- (31) Wan, K.; Yu, Z. P.; Liu, Q. B.; Piao, J. H.; Zheng, Y. Y.; Liang, Z. X. An ultrathin 2D semi-ordered mesoporous silica film: Co-operative assembly and application. *RSC Adv.* **2016**, *6*, 75058-75062.
- (32) Liu, Y.; Chen, F.; Ye, W.; Zeng, M.; Han, N.; Zhao, F.; Wang, X.; Li, Y. High-performance oxygen reduction electrocatalyst derived from polydopamine and cobalt supported on carbon nanotubes for metal–air batteries. *Adv. Funct. Mater.* **2017**, *27*, 1606034.
- (33) Wan, K.; Tan, A. D.; Yu, Z. P.; Liang, Z. X.; Piao, J. H.; Tsiakaras, P. 2D nitrogen-doped hierarchically porous carbon: Key role of low dimensional structure in favoring electrocatalysis and mass transfer for oxygen reduction reaction. *Appl. Catal. B Environ.* **2017**, *209*, 447-454.

- (34) Huang, F.; Sui, Y. W.; Wei, F. X.; Qi, J. Q.; Meng, Q. K.; He, Y. Z. Ni₃S₄ supported on carbon cloth for high-performance flexible all-solid-state asymmetric supercapacitors. *J. Mater. Sci.: Mater. Electron.* **2018**, *29*, 2525-2536.
- (35) Zhang, Z.; Wang, Q.; Zhao, C.; Min, S.; Qian, X. One-step hydrothermal synthesis of 3D petal-like Co₉S₈/rGO/Ni₃S₂ composite on nickel foam for high-performance supercapacitors. *ACS Appl. Mater. Interfaces* **2015**, *7*, 4861-4868.
- (36) Lv, J.; Cheng, Y.; Liu, W.; Quan, B.; Liang, X.; Ji, G.; Du, Y. Achieving better impedance matching by a sulfurization method through converting ni into NiS/Ni₃S₄ composites. *J. Mater. Chem. C* **2018**, *6*, 1822-1828.
- (37) Zhang, B.; Zheng, X.; Voznyy, O.; Comin, R.; Bajdich, M.; Garcia-Melchor, M.; Han, L.; Xu, J.; Liu, M.; Zheng, L.; Garcia de Arquer, F. P.; Dinh, C. T.; Fan, F.; Yuan, M.; Yassitepe, E.; Chen, N.; Regier, T.; Liu, P.; Li, Y.; De Luna, P.; Janmohamed, A.; Xin, H. L.; Yang, H.; Vojvodic, A.; Sargent, E. H. Homogeneously dispersed multimetal oxygen-evolving catalysts. *Science* **2016**, *352*, 333-337.
- (38) Görlin, M.; Chernev, P.; Ferreira de Araújo, J.; Reier, T.; Dresp, S.; Paul, B.; Krähnert, R.; Dau, H.; Strasser, P. Oxygen evolution reaction dynamics, faradaic charge efficiency, and the active metal redox states of Ni–Fe oxide water splitting electrocatalysts. *J. Am. Chem. Soc.* **2016**, *138*, 5603-5614.
- (39) Wang, H. Y.; Hsu, Y. Y.; Chen, R.; Chan, T. S.; Chen, H. M.; Liu, B. Ni³⁺-induced formation of active NiOOH on the spinel Ni-Co oxide surface for efficient oxygen evolution reaction. *Adv. Energy Mater.* **2015**, *5*, 1500091.
- (40) Tahir, M.; Pan, L.; Zhang, R.; Wang, Y. C.; Shen, G.; Aslam, I.; Qadeer, M. A.; Mahmood, N.; Xu, W.; Wang, L.; Zhang, X.; Zou, J. J. High-valence-state NiO/Co₃O₄ nanoparticles on

nitrogen-doped carbon for oxygen evolution at low overpotential. *ACS Energy Lett.* **2017**, *2*, 2177-2182.

(41) Wan, K.; Luo, J.; Zhou, C.; Zhang, T.; Arbiol, J.; Lu, X.; Mao, B. W.; Zhang, X.; Fransaer, J. Hierarchical porous Ni₃S₄ with enriched high-valence Ni sites as a robust electrocatalyst for efficient oxygen evolution reaction. *Adv. Funct. Mater.* **2019**, 1900315.

(42) Zhong, H. X.; Wang, J.; Zhang, Q.; Meng, F.; Bao, D.; Liu, T.; Yang, X. Y.; Chang, Z. W.; Yan, J. M.; Zhang, X. B. In situ coupling FeM (M = Ni, Co) with nitrogen-doped porous carbon toward highly efficient trifunctional electrocatalyst for overall water splitting and rechargeable Zn–air battery. *Adv. Sustain. Syst.* **2017**, *1*, 1700020.

(43) Li, J.; Lu, S.; Huang, H.; Liu, D.; Zhuang, Z.; Zhong, C. Zif-67 as continuous self-sacrifice template derived NiCo₂O₄/Co,N-CNTs nanocages as efficient bifunctional electrocatalysts for rechargeable Zn–air batteries. *ACS Sustain. Chem. Eng.* **2018**, *6*, 10021-10029.

(44) Li, Z.; He, H.; Cao, H.; Sun, S.; Diao, W.; Gao, D.; Lu, P.; Zhang, S.; Guo, Z.; Li, M.; Liu, R.; Ren, D.; Liu, C.; Zhang, Y.; Yang, Z.; Jiang, J.; Zhang, G. Atomic Co/Ni dual sites and Co/Ni alloy nanoparticles in N-doped porous janus-like carbon frameworks for bifunctional oxygen electrocatalysis. *Appl. Catal. B Environ.* **2019**, *240*, 112-121.

(45) Wan, W.; Liu, X.; Li, H.; Peng, X.; Xi, D.; Luo, J. 3D carbon framework-supported CoNi nanoparticles as bifunctional oxygen electrocatalyst for rechargeable Zn–air batteries. *Appl. Catal. B Environ.* **2019**, *240*, 193-200.

(46) Chen, B.; He, X.; Yin, F.; Wang, H.; Liu, D. J.; Shi, R.; Chen, J.; Yin, H. MO-Co@N-doped carbon (M = Zn or Co): Vital roles of inactive Zn and highly efficient activity toward oxygen reduction/evolution reactions for rechargeable Zn–air battery. *Adv. Funct. Mater.* **2017**, *27*, 1700795.

(47) Li, C.; Liu, H.; Yu, Z. Novel and multifunctional inorganic mixing salt-templated 2D ultrathin Fe/Co-N/S-carbon nanosheets as effectively bifunctional electrocatalysts for Zn–air batteries. *Appl. Catal. B Environ.* **2019**, *241*, 95-103.

(48) Yang, L.; Zeng, X.; Wang, D.; Cao, D. Biomass-derived feni alloy and nitrogen-codoped porous carbons as highly efficient oxygen reduction and evolution bifunctional electrocatalysts for rechargeable Zn–air battery. *Energy Storage Mater.* **2018**, *12*, 277-283.

(49) Li, G.; Wang, X.; Fu, J.; Li, J.; Park, M. G.; Zhang, Y.; Lui, G.; Chen, Z. Pomegranate-inspired design of highly active and durable bifunctional electrocatalysts for rechargeable metal–air batteries. *Angew. Chem. Int. Edit.* **2016**, *55*, 4977-4982.

(50) Li, Y.; Gao, J.; Zhang, F.; Qian, Q.; Liu, Y.; Zhang, G. Hierarchical 3D macrosheets composed of interconnected in situ cobalt catalyzed nitrogen doped carbon nanotubes as superior bifunctional oxygen electrocatalysts for rechargeable Zn–air batteries. *J. Mater. Chem. A* **2018**, *6*, 15523-15529.

(51) Cheng, H.; Li, M. L.; Su, C. Y.; Li, N.; Liu, Z. Q. Cu–Co bimetallic oxide quantum dot decorated nitrogen-doped carbon nanotubes: A high-efficiency bifunctional oxygen electrode for Zn–air batteries. *Adv. Funct. Mater.* **2017**, *27*, 1701833.

(52) Liu, P.; Gao, D.; Xiao, W.; Ma, L.; Sun, K.; Xi, P.; Xue, D.; Wang, J. Self-powered water-splitting devices by core-shell NiFe@N-graphite-based Zn–air batteries. *Adv. Funct. Mater.* **2018**, *28*, 1706928.

(53) Wang, H. F.; Tang, C.; Wang, B.; Li, B. Q.; Zhang, Q. Bifunctional transition metal hydroxysulfides: Room-temperature sulfurization and their applications in Zn–air batteries. *Adv. Mater.* **2017**, *29*, 1702327.

(54) Wang, Q.; Lei, Y.; Chen, Z.; Wu, N.; Wang, Y.; Wang, B.; Wang, Y. Fe/Fe₃C@C nanoparticles encapsulated in N-doped graphene–CNTs framework as an efficient bifunctional oxygen electrocatalyst for robust rechargeable Zn–air batteries. *J. Mater. Chem. A* **2018**, *6*, 516-526.

(55) Kashyap, V.; Kurungot, S. Zirconium-substituted cobalt ferrite nanoparticles-supported N-doped reduced graphene oxide as an efficient bifunctional electrocatalyst for rechargeable Zn–air battery. *ACS Catal.* **2018**, *8*, 3715-3726.

(56) Meng, T.; Hao, Y. N.; Zheng, L.; Cao, M. Organophosphoric acid-derived CoP quantum dots@S, N-codoped graphite carbon as a trifunctional electrocatalyst for overall water splitting and Zn–air batteries. *Nanoscale* **2018**, *10*, 14613-14626.

(57) Li, S.; Cheng, C.; Zhao, X.; Schmidt, J.; Thomas, A. Active salt/silica-templated 2d mesoporous FeCo-N_x-carbon as bifunctional oxygen electrodes for zinc–air batteries. *Angew. Chem. Int. Edit.* **2018**, *57*, 1856-1862.

(58) Wang, X. R.; Liu, J. Y.; Liu, Z. W.; Wang, W. C.; Luo, J.; Han, X. P.; Du, X. W.; Qiao, S. Z.; Yang, J. Identifying the key role of pyridinic-N-Co bonding in synergistic electrocatalysis for reversible ORR/OER. *Adv. Mater.* **2018**, *30*, 1800005.

(59) Ren, J. T.; Yuan, G. G.; Chen, L.; Weng, C. C.; Yuan, Z. Y. Rational dispersion of Co₂P₂O₇ fine particles on N,P-codoped reduced graphene oxide aerogels leading to enhanced reversible oxygen reduction ability for Zn–air batteries. *ACS Sustain. Chem. Eng.* **2018**, *6*, 9793-9803.